Phosphoinositide substrates of myotubularin affect voltage-activated Ca^{2+} release in skeletal muscle

Estela González Rodríguez[2], Romain Lefebvre[1], Dóra Bodnár[3], Claude Legrand[1], Peter Szentesi[3], János Vincze[3], Karine Poulard[4], Laszlo Csernoch[3], Anna Buj-Bello[4] and Vincent Jacquemond[1]

[1] UMR CNRS 5534 Centre de Génétique et de Physiologie Moléculaire et Cellulaire, Université Lyon 1, Villeurbanne, France.
[2] Departamento de Fisiología, Genética y Microbiología, Universidad de Alicante, Spain.
[3]Department of Physiology, University of Debrecen, Debrecen, Hungary.
[4] Department of Research and Development, Généthon, INSERM, Evry, France

Running title: Phosphoinositides and E-C coupling

Key words: calcium homeostasis, excitation-contraction coupling, ryanodine receptor, sarcoplasmic reticulum Ca^{2+} release, phosphatidylinositol-phosphate.

Corresponding author:
V. Jacquemond
Centre de Génétique et de Physiologie Moléculaires et Cellulaires
Université Lyon 1, UMR CNRS 5534
Bât. Raphaël Dubois
43 boulevard du 11 novembre 1918
F69622 Villeurbanne, France.
Tel. (33) 4 72 44 81 64
Fax : (33) 4 72 44 79 37
E-mail : vincent.jacquemond@univ-lyon1.fr

ABSTRACT

Skeletal muscle excitation-contraction (E-C) coupling is severely altered in several models of phosphatidylinositol-phosphates (PtdIns*Ps*) phosphatase deficiency thus prompting investigation of the role of PtdIns*P*s in this process. We found that the peak amplitude of voltage-activated Ca^{2+} release was depressed by ~30 % and 50 % in mouse muscle fibers microinjected with a solution containing PtdIns(3,5)P_2 or PtdIns(3)*P*), respectively, the two main substrates of myotubularin phosphatase (MTM1). This occurred with no concurrent alteration in the membrane current signals associated with the DHPR function. In permeabilized muscle fibers, the frequency of spontaneous Ca^{2+} release events was also depressed in the presence of the two MTM1 substrates with no change in the peak amplitude and spatial properties of the events. These results support the possibility that accumulation of MTM1 substrates upon MTM1-deficiency may acutely alter RyR1 function so as to depress voltage-activated SR Ca^{2+} release. Ca^{2+} release was unaffected by MTM1 over-expression and was also unaffected by the PtdIns-3-kinase inhibitor LY2940002 suggesting that the 3-phosphorylated PtdIns lipids active on voltage-activated Ca^{2+} release are inherently maintained at a low inefficient level in normal conditions.

INTRODUCTION

The function of phosphoinositides had for a long time remained limited to the possible role of phosphatidylinositol 4, 5-bisphosphate (PtdIns(4,5)P_2) as a substrate of phospholipase C to produce inositol-trisphosphate (Ins(1,4,5)P_3) and diacylglycerol. The last decade has seen a remarkable expansion of the concept so as to now include the role of PtdIns*P*s phosphorylated in the 3-OH position, which control a wide array of cellular functions including membrane trafficking, cytoskeleton remodeling, protein docking, membrane transport … (for review see (1)) and numerous studies have also revealed the fundamental role of PtdIns*P*s in regulating ion channels activity (see for reviews (2,3)).

Skeletal muscle cells contract in response to depolarizing changes of their plasma membrane voltage: action potentials fired at the end-plate of the muscle fibers propagate throughout the transversal (t-) tubule system: coupling between membrane depolarization and contraction occurs within the triad regions where one t-tubule faces 2 terminal cisternae of sarcoplasmic reticulum (SR). There, depolarization changes the conformation of the dihydropyridine receptor (DHPR, the Cav1.1 protein, the voltage-sensing component of the system) which opens up the SR calcium release channel (type 1 ryanodine receptor, RyR1) through protein-protein conformational coupling. Upon membrane repolarization, RyR1 channels close, muscle relaxation occurs due to cytosolic Ca^{2+} extrusion driven by the SR Ca^{2+} pump.

This basic functional scheme is either known or presumed to be controlled, regulated or modulated by a wide array of accessory proteins and messenger molecules (for review, see (4)). The possible role of PtdIns*P*s in the regulation of Ca^{2+} homeostasis and E-C coupling in muscle remained elusive until the recent years. Indeed if one excludes the controversies related to the possible role of the Ins(1,4,5)P_3 pathway (e.g. (5)) only a few rare studies in the 90s suggested that PtdIns(4,5)P_2 could affect the SR Ca^{2+} release process (6-8). However recent data from transgenic models of PtdIns*P*-phosphatase deficiency, specifically MTM1 (myotubularin) and parent proteins (MTMRs, "myotubularin and myopathy related" phosphatases, see (9)) provided completely unanticipated insights into the field : in human, more than 200 mutations of the gene encoding MTM1 are associated with X-linked myotubular myopathy (see (10)), characterized by very severe muscle weakness and consequent fatal outcome, often within the weeks following birth (11). The link between MTM1 deficiency and muscle weakness remained obscure until muscle fibers from MTM1-deficient mice were shown to suffer from a critically defective E-C coupling process (12). Concurring data from a MTM1-deficient zebrafish model were provided by Dowling et al. (13). In mouse, MTM1-deficient muscle fibers yield defects in the internal membrane system structure and organization, reduced levels of DHPR and RyR1 and a strong decrease in the amplitude of voltage-activated cytosolic Ca^{2+} signals. This functional alteration is certainly the direct cause of muscle weakness in the affected patients. Results by Al Qusairi et al. (12) also demonstrated that SR Ca^{2+} content and cytosolic Ca^{2+} removal capabilities are unaltered in MTM1-deficient muscle fibers. At the functional level, the disease status appears thus to specifically affect the SR Ca^{2+} release process.

The internal membrane architecture defects may contribute to this alteration but are likely not the sole explanations: inner structure alterations are common features of several types of muscle disorders and are already observed in young MTM1-deficient mice which have limited defects in muscle function (12). Furthermore, MTMR14 deficiency in zebrafish is also associated with defective E-C coupling, but without the inner-membrane-systems architecture defects observed in absence of MTM1 (14). The reduction in the level of RyR1 would also, intuitively, be expected to play a role in muscle weakness, but actually the question of how much of the normal RyR1 content is necessary to sustain E-C coupling in

muscle is far from clearly established. It is important to point out in this respect that several human muscle diseases due to *RYR1* mutations have been shown to be associated with a more severe reduction in RyR1 than observed under the conditions of MTM1-deficieny; the fact that severe RyR1 reduction in these cases was associated with a much lesser impact on muscle function and life expectancy (15-18) seems to indicate that this may not be the critical issue determining the severity of myotubular myopathy.

One obvious possibility is that the E-C coupling defect results from altered PtdIns*P*s metabolism due to the loss of MTM1 PtdIns*P*-phosphatase activity. It is supported by results from Shen et al. (19) showing that loss of another PtdIns*P*-phosphatase (MTMR14) is responsible for alterations of intracellular Ca^{2+} homeostasis in muscle, attributable to defective regulation of RyR1 channel activity by PtdIns*P*s. Recent data also indicate that muscle weakness associated with aging may be due to altered Ca^{2+} homeostasis because of a reduced level of MTMR14 (20). This trend of data thus tends to suggest a role for PtdIns*P*s in the regulation of skeletal muscle Ca^{2+} homeostasis and E-C coupling under normal conditions and a role for alteration of this regulation in certain muscle diseases. We looked here for direct evidence that PtdIns*P*s are physiologically involved in the regulation of Ca^{2+} and E-C coupling in normal muscle. We demonstrate that MTM1 main PtdIns*P*-substrates inhibit the function of E-C coupling while maneuvers intended to reduce the level of these 3-OH phosphorylated PtdIns have no effect.

MATERIALS AND METHODS

Ethical approval

All experiments and procedures were in accordance with the guidelines of the local animal ethics committee of University Lyon 1 and University of Debrecen, of the French Ministry of Agriculture (87/848) and of the European Community (86/609/EEC).

In vivo transfection

An expression plasmid encoding wild-type mouse MTM1 fused N-terminally to mCherry was constructed using the pmCherry-C1 vector (Clontech, Mountain View, CA, USA). Swiss OF1 male mice 1-2 months-old were used. Transfection was performed in the *flexor digitorum brevis* (fdb) and interosseus muscles of the animals. Details of the procedure used for *in vivo* electroporation are given in the Supporting Material. Experimental observations and measurements were carried out 7-10 days later.

Preparation of isolated muscle fibers

Single fibers were isolated from the *fdb* and interosseus muscles from mouse using a previously described procedure (21). In brief, mice were killed by cervical dislocation before removal of the muscles. Muscles were treated with collagenase (Sigma, type 1) for 60 min at 37 °C. Single fibers were then obtained by triturating the muscles within the experimental chamber. They were dispersed on the glass bottom of a 50 mm wide culture μ-dish (Biovalley, Marne la Vallée, France). For intracellular Ca^{2+} measurements under voltage-clamp conditions, fibers were first partially insulated with silicone grease as described previously (21); in brief fibers were embedded within silicone so that only a portion of the fiber extremity was left out of the silicone. Under these conditions fibers remained well maintained on the bottom of the chamber and this allowed whole-cell voltage clamp to be achieved on the silicone-free extremity of the fiber. Once partially embedded within silicone,

indo-1 or fluo-4 was introduced into the myoplasm through local pressure micro-injection with a micropipette containing 1 mM of the dye. Indo-1 was dissolved in the standard intracellular-like solution (see Solutions) whereas fluo-4 was dissolved in a solution containing 100 mM EGTA and 40 mM $CaCl_2$. Details regarding the use of EGTA are given in the Supporting Material. Microinjection was always performed within the silicone-embedded part of the fiber, away from the silicone-free end portion under study. Following diffusion and equilibration within the cytoplasm, this was believed to achieve a final cytoplasmic concentration or indo-1 or fluo-4 within the 100 μM range and of EGTA within the 10 mM range, respectively (for details concerning micro-injections see (22)). Experiments were usually performed on fibers from the *fdb* muscle; only when testing the effect of MTM1 over-expression were a few control and MTM1-positive fibers from interosseus muscles used. For all experimental situations, control fibers (either untreated with the tested reagent or non-expressing the tested transfected gene) were always from the same muscles as the tested fibers. All experiments were performed at room temperature (20-22 °C).

Electrophysiology

An RK-400 patch-clamp amplifier (Bio-Logic, Claix, France) was used in whole-cell voltage-clamp configuration. Fibers were bathed in the TEA-containing extracellular solution (see Solutions). Command voltage pulse generation was achieved with an analog-digital converter (Digidata 1440A, Axon Instruments, Foster City, CA) controlled by pClamp 9 software (Axon Instruments). Voltage-clamp was performed with a microelectrode filled with the intracellular-like solution (see Solutions). The tip of the microelectrode was inserted through the silicone, within the insulated part of the fiber. Analog compensation was systematically used to decrease the effective series resistance. Membrane depolarizing steps were applied from a holding command potential of -80 mV, unless otherwise specified. Removal of the linear leak and capacitive components of the current changes elicited by a depolarizing pulse was achieved using previously described procedures (23, 24). For the short (20 ms-long) pulses, adequately scaled control current records elicited by 20 ms-long hyperpolarizing pulses of 20 mV from the holding potential were subtracted from the current elicited by the test depolarizing pulses. The amount of charge moved during a test pulse was measured by integrating the positive *on* portion of the corrected test current record. Values for *on* charge and for Ca^{2+} current amplitude were normalized to the capacitance of the fiber.

For Ca^{2+} current measurements taken in response to 0.5 s-long depolarizing pulses, the voltage dependence of current density was determined by fitting individual series of data points from each cell with the following equation:

$$I(V)=G_{max}(V-V_{rev})/\{1+\exp[(V_{0.5}-V)/k],$$

where $I(V)$ is the peak current density at the command potential V, G_{max} is the maximum conductance, V_{rev} is the apparent reversal potential, $V_{0.5}$ is the half-activation potential and k is the steepness factor.

Fluorescence measurements in voltage-clamped fibers

Indo-1 fluorescence was measured on an inverted Nikon Diaphot epifluorescence microscope equipped with a commercial optical system allowing the simultaneous detection of fluorescence at 405 nm (F405) and 485 nm (F485) by two photomultipliers (IonOptix, Milton, MA), upon 360 nm excitation. Background fluorescence at both emission wavelengths was measured next to each fiber tested and was then subtracted from all measurements.

Confocal fluorescence measurements were done using a Zeiss LSM 5 Exciter confocal microscope equipped with a × 63 oil immersion objective (numerical aperture 1.4). Fluo-4 excitation was provided by the 488 nm line of an argon laser and a 505-600 nm band pass

filter was used on the detection channel. For detection of m-Cherry fluorescence the excitation was from the 543 nm line of a HeNe laser and fluorescence was collected above 560 nm. Intracellular [Ca^{2+}]-related fluorescence changes were imaged by using the line-scan mode of the system with the line parallel to the longitudinal fiber axis. The majority of images were taken with a scanning frequency of 1.15 ms per line. Image processing and analysis was performed using Image/J (NIH, USA) and Microcal Origin (Microcal Software Inc., Northampton, MA).

[Ca^{2+}] and Ca^{2+} release calculation in intact fibers

For indo-1 fluorescence signals, the standard ratio method was used with the parameters: $R = F_{405}/F_{485}$, with R_{min}, R_{max}, K_D and β having their usual definitions. Results were either expressed in terms of indo-1 % saturation or in actual free Ca^{2+} concentration; in vivo values for R_{min} and β were measured using procedures previously described previously (21). R_{max} was determined at the end of the experiments after damaging the fiber under study with a thin needle until complete contracture. An estimation of the Ca^{2+} release flux underlying the calculated global [Ca^{2+}] transients was performed according to a previously described procedures (25, 26). Details of the procedure used for Ca^{2+} release calculation are given in the Supporting Material. Fluo-4 changes in fluorescence were expressed as F/F_0 where F_0 is the resting (or baseline) fluorescence level. Changes in [Ca^{2+}] were calculated from the fluo-4 signals using the previously described pseudo-ratio equation (27) assuming a basal [Ca^{2+}] of 100 nM and a K_d of fluo-4 for Ca^{2+} of 1 μM (28). No correction was made for the fluo-4 binding kinetics.

The voltage dependence of activation of Ca^{2+} release was fitted with a Boltzmann function:

$$d[Ca]_T/dt(V) = d[Ca]_T/dt\,max/\{1+\exp[(V_{0.5}-V)/k],$$

where $d[Ca]_T/dt(V)$ is the peak Ca^{2+} release at command voltage V, $d[Ca]_T/dt\ max$ is the maximum peak Ca^{2+} release, $V_{0.5}$ is the voltage of half-activation and k is the steepness factor.

Measurements of elementary Ca^{2+} release events (ECREs) in permeabilized muscle fibers

Isolated mouse skeletal muscle fibers from the *fdb* were permeabilized with saponin and loaded with 0.1 mM fluo-3 using previously described experimental solutions and procedures (29). In brief, fibers were bathed in a relaxing solution (see Solutions) containing 0.002% saponin for 2–3 min. Permeabilization of the surface membrane was monitored by imaging the fluorescence of fluo-3 present at a concentration of 0.1 mM in the solution. This solution was then replaced by the recording solution (see Solutions). Images were captured with a Zeiss LSM 510 LIVE confocal microscope (Zeiss, Oberkochen, Germany) equipped with a 40× oil immersion objective (NA=1.3). Fluo-3 was excited with the 488-nm line of an argon laser and the emitted fluorescent light was measured at wavelengths > 505 nm. 15 minutes following application of the recording solution, eight consecutive series of 200 512×512 (x,y) images captured every 67 ms were collected in each tested fiber. Test experiments were carried in the presence of 0.1 mM of a given PtdIns$P$ species (diC8, Echelon Biosciences Inc.) in the recording solution. For each series of test measurements in fibers bathed in the presence of a given PtdIns$P$, a parallel series of control measurements (with no PtdIns$P$) was made using fibers isolated from the same muscles. For analysis, results from a given PtdIns$P$ condition were compared to those from the corresponding group of control fibers. Measurements with PtdIns(3,5)P_2, PtdIns(3)P) and (PtdIns(5)P were performed within the same series of experiments whereas measurements with PtdIns were performed 6 months later.

ECRE detection and analysis were performed using modified methods and algorithms described previously by Szabo et al. (30). In brief, the region of the fiber and the background

were defined on the first image of each series. Background was selected as part of the image, outside of the fiber (i.e. from spatial positions where no dye was present). Fluorescence intensities from pixels in this area were averaged and this average was then subtracted from all pixels in the given image. Next the fluorescence intensity pattern corresponding to the Z-lines was removed. To identify the Z-lines the frequency spectrum in each line of all images was calculated using a fast Fourier transform. Images were de-noised using the stationary wavelet transform based method described by Szabo et al. (30) before calcium release events were detected. Finally, the amplitude and the full width at half maxima (FWHM) – determined both perpendicular ($FWHM_x$) and parallel ($FWHM_y$) in respect to the Z-lines – of the sparks were calculated. Bleaching correction was performed on all images: for this, the change in fluorescence intensity of each pixel in time was calculated; it was then normalized using the low-frequency components after 4 rounds of stationary wavelet transform (F_4 as described in Equation (2) by Szabo et al. (30)).

To determine the event frequency for a given condition the number of events on all images from a 200 series was counted. Events that occurred on consecutive images at the same location were counted as a single event. Numbers were normalized to total recording time and fiber area and averaged over the fibers. To generate the images in the Figures, all images in the series of 200 images were merged. To this end, sparks (square areas containing the sparks) were removed from the images and then the images were averaged. This averaged image was used as the F_0 image for normalizing (calculating the ratio image pixel by pixel) each image in the series. These normalized ($\Delta F/F_0$) images were then summed. If a spark at a given location appeared more than once in the series only one appearance, the one with the largest amplitude, was included into the merged image.

Solutions

The extracellular solution used for whole-cell voltage-clamp contained (in mM) 140 TEA-methanesulfonate, 2.5 $CaCl_2$, 2 $MgCl_2$, 10 TEA-HEPES and 0.002 tetrodotoxin. In certain series of measurements 4-aminopyridine was also present at 1 mM. The intracellular-like solution for whole-cell voltage-clamp contained (in mM) 120 K-glutamate, 5 Na_2-ATP, 5 Na_2-phosphocreatine, 5.5 $MgCl_2$, 5 glucose, 5 HEPES. For indo-1 fluorescence measurements, the dye was present at 1 mM in the injected intracellular-like solution. PtdIns*P*s (diC8, Echelon Biosciences Inc.) were present at 1 mM in the injected solution. LY294002 (Echelon Biosciences Inc.) was prepared in DMSO at a concentration of 10 mM and diluted at 1 mM in the injection solution; DMSO at the same concentration was injected in the control fibers from that series of measurements. For confocal line-scan fluo-4 fluorescence measurements under voltage-clamp conditions, the injected solution contained (in mM) 100 EGTA, 40 $CaCl_2$ and 1 fluo-4. For measurements of ECREs in permeabilized fibers, the relaxing solution contained (in mM) 125 K-glutamate, 10 HEPES, 1 EGTA, 6 $MgCl_2$, 5 Na_2-ATP, 10 Na-phosphocreatine, 10 glucose, 0.13 $CaCl_2$ and the recording solution contained (in mM) 95 K_2SO_4, 10 HEPES, 1 EGTA, 6 $MgCl_2$, 5 Na_2-ATP, 10 Na-phosphocreatine, 10 glucose, 0.13 $CaCl_2$, respectively. All solutions were adjusted to pH 7.20.

Statistics

Least-squares fits were performed using a Marquardt-Levenberg algorithm routine included in Microcal Origin (Originlab, Northampton, MA). Data values are presented as means ± S.E.M. for *n* fibers. Statistical significance was determined using a Student's t-test: *$p \leq 0.05$, **$p \leq 0.01$, ***$p \leq 0.001$.

RESULTS

PtdIns(3,5)P2 and PtdIns(3)P depress voltage-activated Ca^{2+} release

Since MTM1 deficiency produces a severe impairment of E-C coupling (12) we were specifically interested in the effect of substrates and products of its phosphatase activity. Soluble forms of PtdIns(3,5)P_2, PtdIns(3)*P*, PtdIns(5)*P* or PtdIns were thus micro-injected in separate batches of single isolated muscle fibers and intracellular Ca^{2+} was measured under voltage-clamp conditions. PtdIns*P*s injection was performed so as to reach a final concentration expected to be within the 100 µM range, matching the maximum levels of PtdIns*P*s shown to affect [^{3}H] ryanodine binding to SR as well as single channel activity of RyR1 in bilayer (19). Mean resting [Ca^{2+}] did not differ between control fibers (0.16 ± 0.02 µM, n=16) and any of the PtdIns*P*s-injected fiber group, but was significantly elevated in fibers injected with either PtdIns(3,5)P_2 (0.21 ± 0.02 µM, n=8) or PtdIns(3)*P* (0.20 ± 0.02 µM, n=8) as compared to fibers injected with PtdIns(5)*P* (0.14 ± 0.01 µM, n=7) or PtdIns (0.12 ± 0.02 µM, n=6).

In order to evaluate the effect of the different PtdIns*P*s on the properties of Ca^{2+} transients and Ca^{2+} release, fibers were stimulated by a voltage-clamp protocol consisting in successive 20 ms-long depolarizing pulses of increasing amplitude from -80 mV (Fig. S1A in the Supporting Material). This protocol was repeated 5 times in each fiber and the traces were averaged. Figure S1B shows an illustrative average indo-1 saturation trace obtained in a control fiber in response to this protocol; Fig. S1C shows the corresponding Ca^{2+} release trace calculated as described in Materials and Methods while Fig. S1D shows an expanded view of a portion of that same trace centered on the last transient. Figure 1 shows mean indo-1 saturation traces obtained in response to this protocol in the different batches of fibers. The grey shading superimposed to each trace corresponds to the S.E.M. There was no obvious alteration of the qualitative kinetic properties of the transients in the presence of any of the PtdIns*P*s. However the peak amplitude was depressed in the presence of PtdIns(3)*P* and, to a lesser extent also in the presence of PtdIns(3,5)P_2. The graphs on the right in Fig.1 report the voltage dependence of the mean value for peak Ca^{2+} release in each corresponding condition. The voltage dependence of peak Ca^{2+} release was fitted in each fiber with a Boltzmann function. Figure S2 in the Supporting Material shows the corresponding mean values for maximum peak Ca^{2+} release (d[Ca]$_T$/dt max), voltage of half-activation ($V_{0.5}$) and steepness factor (k); as compared to control fibers, maximum Ca^{2+} release was depressed by 40 and 30 % in the presence of PtdIns(3)*P* ($p<0.001$) and PtdIns(3,5)P_2 ($p=0.02$), respectively, whereas the steepness factor was slightly but significantly enhanced in the presence of PtdIns(3,5)P_2 ($p=0.001$) and PtdIns(5)*P* ($p=0.03$). It is worth stressing that indo-1 is a rather high-affinity Ca^{2+} dye with limited kinetic properties precluding fully reliable detection of large fast changes in [Ca^{2+}]. Still, when used in combination with voltage-clamp, the possibility to measure Ca^{2+} transients in response to small levels of depolarization for which the dye remains far from saturation limits the high-saturation hazardous effects. In other words indo-1 limitations should in no case affect the qualitative effects of PtdIns*P*s observed here but the exact extent of inhibition of Ca^{2+} release by PtdIns(3)*P* and PtdIns(3,5)P_2 may have been somewhat underestimated.

In order to test whether the function of the DHPR was affected and potentially responsible for the above described effects we analyzed the membrane current records taken during these experiments. Figure 2B shows the portions of interest of the mean membrane current trace from the control fibers in response to the successive pulses (Fig. 2A); in each fiber the linear capacitive and resistive components of the current were removed as described in Materials and Methods. We measured the integral of the positive portion of the corrected

current transient at the onset of the pulse as an approximation of the *on* intramembrane charge (31); although this estimation is to some extent corrupted by the inward current that develops for voltages more positive than -10 mV, any serious alteration of charge movement by one of the PtdIns*P* compounds should be revealed by this analysis. In parallel, the membrane current at the end of the pulse was used to estimate the Ca^{2+} channel activity of the DHPR during these experiments.

The different panels in Fig. 2C show the voltage dependence of the approximated mean *on* charge (top) and of the mean membrane current at the end of the depolarizing pulse (bottom) in each group of PtdIns*P*-injected fibers; mean values from control fibers are reported in each panel as filled symbols. Statistical comparison of each mean value with the control mean value at a given membrane voltage showed no significant alteration of both parameters in the different groups of PtdIns*P*-injected fibers, throughout the voltage range.

An additional specific series of membrane current measurements was also carried out in fibers injected with the two PtdIns*P*s that were found to reduce Ca^{2+} release; for these measurements the injected solution contained 50 mM EGTA and fibers were stimulated by 0.5 s-long depolarizing pulses of increasing amplitude. Again no severe alteration of the Ca^{2+} current was observed (not illustrated): fitting the individual *I(V)* curves with a modified Boltzmann equation gave mean values for G_{max}, V_{rev}, $V_{1/2}$ and k of 86 ± 9, 110 ± 15 and 59 ± 6 S/F, 82 ± 3, 75 ± 5 and 84 ± 4 mV, 17 ± 1, 24 ± 3 and 14 ± 2 mV, 6.8 ± 0.3, 8 ± 1 and 6.1 ± 0.3 mV in control (n=17), PtdIns(3,5)P_2 injected (n=10) and PtdIns(3)*P* injected fibers (n=10), respectively. The only significant change was a 7 mV right-shift in the voltage-dependence of current activation in the PtdIns(3,5)P_2 injected fibers (p=0.04).

While testing the effect of PtdIns*P*s on Ca^{2+} transients, we questioned the possibility that voltage-dependent inactivation of Ca^{2+} release would be affected. To test for this, we measured indo-1 transients in response to a pair of 20-ms long pulses to -20 and 0 mV from increasing levels of holding potential. The two pulses were used in order to ensure that heavy saturation of indo-1 for the largest pulse would not hinder detection of a decrease in the Ca^{2+} transient amplitude when changing the holding potential towards more depolarized levels. Figure S3A-B in the Supporting Material shows the pulse protocol and the corresponding mean (±S.E.M.) indo-1 saturation traces obtained in control fibers. In each fiber the peak Ca^{2+} transient amplitude calculated from the indo-1 signal was normalized to the initial value measured from the holding potential of -80 mV. We found no indication that any of the four tested PtdIns*P*s affected the inactivation process; this is illustrated in Fig. S3C which shows the mean normalized peak amplitude of the Ca^{2+} transient *versus* the holding potential in the different groups of fibers. Fitting a Boltzmann function to the data in each fiber gave mean values for half-inactivation voltage and steepness factor that did not differ between control fibers and any of the four groups of PtdIns*P*s-injected fibers.

PtdIns(3,5)P_2, PtdIns(3)P and PtdIns(5)P depress the frequency of elementary Ca^{2+} release events (ECREs) in permeabilized muscle fibers

Measurement of spontaneous ECREs in permeabilized muscle fibers provides a way to study the functional properties of the ryanodine receptor in its native environment, freed from the DHPR control (e.g. (32, 33)). We used this approach to test whether PtdIns*P*s would directly affect RyR-mediated Ca^{2+} release activity and get insights into the underlying mechanism. Spontaneous ECREs were measured using fast confocal (x,y) imaging in fibers equilibrated with a given PtdIns*P* and properties of the events were compared to those of

fibers from the same muscles equilibrated with the standard experimental solution. Figure 3A shows an illustrative (*x*,*y*) confocal record of fluo-3 fluorescence from one fiber in each group. Each frame represents the cumulated ECRE activity recorded during a series of 200 consecutive images, covering a period of approximately 13 s. There was a substantial reduction of the number of detected ECREs in the fibers equilibrated with PtdIns(3,5)P_2, PtdIns(3)*P* and PtdIns(5)*P*, the effect being most important with PtdIns(3,5)P_2. Figure 3B shows the mean values for the measured parameters. ECRE frequency was strongly depressed in the presence of each of the three tested phosphorylated forms of PtdIns*P* with the drop amounting 98 % in the presence of PtdIns(3,5)P_2. The mean ECRE amplitude was slightly but significantly increased in the presence of PtdIns(5)*P* whereas the FWHM along both the *x* and *y* direction was depressed by ~10 % in the presence of PtdIns(3,5)P_2. Altogether, the tested PtdIns*P*s appeared to modestly, if any, affect the individual ECRE amplitude and spatial properties while severely impairing the occurrence of the events.

LY2940002 does not affect voltage-activated Ca^{2+} release

As results from Ca^{2+} transients in intact fibers suggested that accumulation of PtdIns(3,5)P_2 and/or PtdIns(3)P is capable of reducing voltage-activated Ca^{2+} release, it was of specific interest to explore the effect of manoeuvres intended to reduce the endogenous level of these compounds. For this, we first used LY294002, a classical pharmacological inhibitor of the different classes of PtdIns 3-kinases. Figure 4 compares indo-1 Ca^{2+} transients measured in a batch of control fibers and fibers injected with LY294002 so the final intracellular concentration was expected to be in the 0.1 mM range, well in the range expected to effectively block all classes of PtdIns 3-kinases (e.g. (34)). Fibers were subjected to the same voltage-clamp stimulation protocol as in Fig. 1. The left panels in Fig. 4 show the mean (± S.E.M.) indo-1 saturation trace from the control (DMSO-injected) and from the LY294002-injected fibers and the graph on the right shows the corresponding voltage-dependence of peak Ca^{2+} release. Presence of the inhibitor clearly had no effect on Ca^{2+} release.

Over-expression of MTM1 does not affect voltage-activated Ca^{2+} release

PtdIns(3,5)P_2 and PtdIns(3)*P* are the main substrates of the PtdIns*P* phosphatase MTM1. An alternative possibility for reducing the level of these two PtdIns*Ps* was thus to over-express MTM1; this was also of particularly strong interest since loss of activity of this phosphatase is responsible for severe pathological E-C coupling defects (12). Figure 5 shows the expression pattern of a mCherry-tagged version of MTM1 expressed in a *fdb* muscle fiber, following *in vivo* transfection (see Material and Methods). Figure 5A-C illustrates the facts that mCherry-MTM1 was distributed throughout the entire volume of the fibers and, interestingly, that the fluorescence yielded a clear transversally striated component forming double-rows spaced by ~2 µm, reminiscent of the triadic region. This was confirmed by co-localization of the mCherry fluorescence with that of t-tubule stained with di-8 anepps (Fig. 5D-F). Figure 6 shows the effect of exogenous MTM1 expression on voltage-activated Ca^{2+} release measured with indo-1. Figure 6B shows mean (± S.E.M.) indo-1 saturation traces obtained from 11 control fibers and 11 mCherry-MTM1 expressing fibers in response to the pulse protocol shown in Fig. 6A; the corresponding voltage dependency of peak Ca^{2+} release is shown in Fig. 6C. Although there was a tendency for a slight reduction in peak Ca^{2+} release in the fibers over-expressing MTM1 as compared to control fibers, the difference was not statistically significant. Fitting a Boltzmann function to the data in each fiber gave mean values for maximum peak Ca^{2+} release, voltage of half-activation and steepness factor of 32.5 ± 3 µM.ms^{-1}, -7.2 ± 1 mV, 6.8 ± 0.2 mV and 28.2 ± 3 µM.ms^{-1}, -5.6 ± 1 mV, 6.5 ± 0.4 mV in control and MTM1-over-expressing fibers, respectively.

Indo-1 is a high affinity dye that gets heavily saturated for large levels of step depolarization, a situation that could be thought to hamper detection of a putative enhancing effect of MTM1 over-expression on Ca^{2+} release; in order to make sure, Ca^{2+} transients from transfected fibers were also measured with fluo-4 in the presence of a high concentration of EGTA (see Material and Methods). Figure S4B in the Supporting Material shows the mean (± S.E.M.) fluo-4 transient evoked by a 0.5 s-long depolarization from -80 mV to +30 mV (Fig. S4A) in control fibers (n=5) and in fibers expressing mCherry-MTM1 (n=7); Fig. S4C shows the corresponding Ca^{2+} release traces. In agreement with the indo-1 data, there was no indication that over-expression of MTM1 affected Ca^{2+} release.

The possibility that the mCherry tag could somehow affect the activity of MTM1 so as to preclude a functional outcome was tested by measuring Ca^{2+} transients in fibers co-transfected with a plasmid encoding tag-free MTM1 and a plasmid encoding EGFP. Control experiments with fibers co-transfected with mCherry-MTM1 and EGFP showed that 92 % of fibers expressing EGFP also yielded the mCherry fluorescence signal. Still, under these conditions indo-1 Ca^{2+} transients evoked by the same protocol as in Fig. 6 were very similar in EGFP-negative and EGFP-positive fibers (not illustrated): fitting a Boltzmann function to the peak Ca^{2+} release *versus* voltage data in each fiber gave mean values for maximum peak Ca^{2+} release, voltage of half-activation and steepness factor of 22.2 ± 2 $\mu M.ms^{-1}$, -12.1 ± 3 mV, 6.6 ± 0.4 mV and 20.6 ± 2 $\mu M.ms^{-1}$, -8.3 ± 1.4 mV, 6.0 ± 0.3 mV in control (n=10) and EGFP-positive fibers (n=10), respectively. For an unclear reason peak Ca^{2+} release values in this batch of fibers were somewhat lower than usual but still, none of the Boltzmann parameters significantly differed between the two groups of fibers. Finally, in another series of experiments, we tested the possibility that the presence of exogenous MTM1 could affect Ca^{2+} release under more stringent conditions of muscle function: for this, control and mCherry-MTM1 expressing fibers were challenged by 20 successive trains of 20, 10 ms-long depolarizing pulses from -80 to +20 mV at 2 Hz, applied every 20 s. Figure S5A in the Supporting Material shows the voltage-clamp pulse protocol while Fig. S5B shows indo-1 saturation traces recorded in a control fiber in response to the first (left) and last (right) train of depolarizing steps. Figure S5C shows the time course of the relative peak amplitude of the indo-1 Ca^{2+} transient in response to the 1^{st}, 10^{th} and 20^{th} pulse in each train over the course of the experiment in control fibers (left, n=10) and in mCherry-MTM1 positive fibers (n=8). In each fiber, the peak amplitude of the 1^{st}, 10^{th} and 20^{th} Ca^{2+} transient was normalized to the corresponding value during the first train. Peak $[Ca^{2+}]$ progressively decreased along the series of 20 trains, but in a manner that did not differ between control and MTM1 over-expressing fibers.

DISCUSSION

The present work provides insights into a so-far unexplored aspect of the E-C coupling function that has direct relevance to a fatal muscle disease. Indeed, the recent discovery that myotubular myopathy is associated with a severe alteration of Ca^{2+} release has highlighted the potentially critical role of PtdIns*P*s metabolism in the maintenance and/or regulation of this process. Details of how PtdIns*P*s are involved in E-C coupling remain though very mysterious.

We show that intracellular application of either PtdIns(3,5)P_2 or PtdIns(3)*P* depresses global voltage-activated Ca^{2+} release in intact muscle fibers. The effect does not seem to be associated with an alteration of the global cytosolic Ca^{2+} removal capabilities of the fibers as

the decay phase of the transients after the end of the pulses suffered no gross alteration in the injected fibers. Conversely we also show that two experimental strategies intended to reduce the level of these two 3-OH phosphorylated PtdIns have no effect on Ca^{2+} release, suggesting that they are maintained at an ineffective low-level in regard to this effect, in normal conditions.

Evidence for a role of PtdIns*P*s in the regulation of muscle Ca^{2+} homeostasis and/or E-C coupling is sparse: mainly, measurements of single RyR channel activity, Ca^{2+} release from SR vesicles and tension from skinned fibers suggested that PtdIns(4,5)P_2 has the potency to activate RyR1 (6, 7, 35) but no clear physiological correlate was ever provided. Our interest here was more specifically focused on the PtdIns*P*s species that are substrates or hydrolyzed products of MTM1. In regard to these, a set of relevant data was collected by Shen et al. (19) indicating that -PtdIns(3,5)P_2 in cultured myotubes resides in the SR, -defects in myotubes Ca^{2+} signalling occur upon perfusion with PtdIns(3,5)P_2, PtdIns(3,4)P_2 or PtdIns(3)*P*, -all PtdIns*P*s bind to RyR1 with PtdIns(5)*P* yielding the highest binding activity, -PtdIns(3,5)P_2, in the 10-100 µM range directly increases the activity of RyR1 as inferred for instance from the increased number of single RyR1 channel open events in reconstituted lipid bilayers. Although of strong relevance to the present issue, these results provided little insight into whether or not, and if so how, PtdIns*P*s actually affect RyR1 function and E-C coupling in the native functional environment of an adult muscle fiber.

Our data provide evidence that physiologically triggered RyR1 function is sensitive to certain PtdIns*P*s: indeed data from intact fibers suggest that intracellular levels of PtdIns(3,5)P_2 or PtdIns(3)*P* in the 100 µM range depress voltage-activated Ca^{2+} release. The question of whether this concentration level of soluble di-C8 forms of PtdIns*P*s tested here has physiological relevance may be raised, though not completely straightforward to answer. PtdIns(3,5)P_2, PtdIns(3)*P* and PtdIns(5)*P* are minor membrane components considered to represent ~0.01, 0.2 and 0.2 % of the total PtdIns plus PtdIns*P*s content in mammalian cells (see (36)). This is 25-500 times less than the estimated level of the more abundant (and more widely studied) PtdIns(4,5)P_2. If uniformly distributed in the cell volume, PtdIns(4,5)P_2 concentration is generally estimated to be within a 10-100 µM range (see for instance (37)). For a muscle fiber assumed to be a cylinder of 25 µm diameter, considering the lipid membrane thickness to be 7 nm, the t-tubule to surface membrane ratio to be 6, the SR volume to represent 5.5 % of total fiber volume (38) and the average inner SR radius to be 10 nm, one can calculate that the volume of surface membrane plus t-system membrane represents ~0.3 % of the total fiber volume while the SR membrane volume represents ~4 % of the total fiber volume. Thus, if distributed uniformly within the surface plus t-system plus SR membrane, the concentration of PtdIns(4,5)P_2 should amount 23 times its concentration in the fiber bulk, that is 0.23-2.3 mM. Accordingly, endogenous levels of PtdIns(3,5)P_2 on one hand and of PtdIns(3)*P* and PtdIns(5)*P* on the other hand should fall into a 0.5-5 and 9-90 µM concentration range, respectively, if distributed uniformly in the volume of these membrane systems. Notice that this neglects the possibility that certain PtdIns*P*s may accumulate in specific areas of a given membrane compartment where they would reach a higher concentration. Nevertheless, despite uncertainties and considering also that PtdIns*P*s resting levels may increase quite substantially upon various types of stimulation (see (36)), the 100 µM concentration of di-C8-PtdIns*P*s used here may not be so far from the range of levels relevant to physiological or patho-physiological conditions.

We also examined the effect of PtdIns*P*s on Ca^{2+} release detected under the form of spontaneous elementary events. Normally, ECREs in mammalian muscle do not occur at a frequency that allows appropriate analysis, under physiological conditions. On the other hand, conditions that substantially increase their frequency, such as here after saponin

permeabilization, allow connection between data measured in vitro (whether from vesicles or from artificial bilayers) and global calcium transients measured in intact muscle fibers. In other words, analysis of ECREs offers a way to address discrepancies of RyR1 function between a full in vitro situation and an - as full as possible - physiological situation. Also considering that the physiological elementary Ca^{2+} release events that build up the global Ca^{2+} transients in mammalian muscle fibers remain still poorly identified, this approach represents the best one can use to address elementary properties of RyR1-mediated Ca^{2+} release in situ. In qualitative agreement with the reduction of peak voltage-activated Ca^{2+} release by PtdIns(3,5)P_2 and PtdIns(3)*P* that we observed in intact fibers we also found that the frequency of spontaneous Ca^{2+} release events was reduced by these two PtdIns*P*s in permeabilized fibers, although in contrast with data from intact fibers PtdIns(5)*P* also was effective under these conditions. According to the ECRE parameters, PtdIns*P*s effect on RyR1-mediated Ca^{2+} release is likely to result from a reduced occurrence of RyR1 channel opening than from an alteration of the channel conductance or of the number of coherently-operating channels involved in a Ca^{2+} release event.

Our data complement the results by Shen et al. (19) showing that di-C8-PtdIns*P*s, at similar concentrations as used here, enhance the activity of RyR1 in vitro. Although these results may not seem intuitively consistent with the present ones, they may not necessarily be contradictory. Notice along this line that even within our study there was no full consistence between the intact and permeabilized fiber data with respect to PtdIns(5)*P* which had no significant effect on voltage-activated Ca^{2+} release while depressing the ECRE frequency. On the other hand, PtdIns(3,5)P_2 was found to be more effective in altering elementary release events than either PtdIns(3)*P* or PtdIns(5)*P*, in line with the observations by Shen et al. (19). Discrepancies may also reflect different levels of complexity of PtdIns*P*s modulation of the RyR1 channel activity when going from the native intact muscle fiber environment with RyR1 under the control of the DHPR as compared to RyR1 spontaneous activity detected in permeabilized fibers under the form of ECREs and again *versus* the in vitro situation in vesicles or bilayer. One may for instance picture the possibility that a target other than RyR1 is involved in the effects at the single fiber level. In this respect, our data tend to exclude the DHPR, as evidenced from analysis of the membrane current measurements. Furthermore, the fact that ECRE, presumed to reflect a DHPR-free activity of RyR1 channels, also yield a depressed activity in the presence of PtdIns*P*s do not favour a role for the DHPR as a critical target. The enhanced PtdIns*P*s-induced RyR1 activity observed in vitro (19) could also be speculated to correspond to a specific effect on the resting level of RyR1 activity in the intact fibers; along such line, it is interesting that despite the reduced amplitude of voltage-activated Ca^{2+} release in fibers injected with PtdIns(3,5)P_2 and PtdIns(3)*P*, resting [Ca^{2+}] level tended to be elevated.

One could have anticipated that under normal conditions, the endogenous level of PtdIns(3,5)P_2 and PtdIns(3)*P* has a chronic effect on Ca^{2+} release that could be overcome by further reducing the level of these molecules. This does not seem to be the case: despite yielding a pattern of expression consistent with the triadic region, over-expression of MTM1 left Ca^{2+} release unchanged. Along the same line, application of a PtdIns 3-kinase inhibitor which would have also been expected to reduce the endogenous level of PtdIns(3,5)P_2 and PtdIns(3)*P* was without effect. Together, these results provide no clue for the existence of a tonic effect of the endogenous PtdIns*P*s on Ca^{2+} release in normal conditions. Interestingly along this line, recent results showed that ectopic expression in muscle of wild-type MTM1 did not induce any detectable signs of muscle alteration with respect to muscle weight, fiber size and isometric force, in agreement with the present results showing that the steps of E-C coupling remained essentially unaffected (39).

Altogether, although full understanding of the details of how PtdIns*P*s affect Ca^{2+} release in situ will necessitate more efforts, our results represent an important first step towards this goal. Also of importance, data highlight the possibility that accumulation of MTM1 substrates has the potency to depress Ca^{2+} release and to thus contribute to the defective E-C coupling in MTM1-deficient conditions (12). The mechanism(s) involved and the actual PtdIns*P*s target(s) still remain speculative. As shown for PtdIns(4,5)P_2 in regard to plasma membrane ion channels, PtdIns(3,5)P_2 and PtdIns(3)*P* may be suggested to exert their effect through a direct interaction with RyR1, and this is supported by the fact that several PtdIns*P*s do bind to RyR1 (19). Alternatively they could also be speculated to favor targeting or translocation of another protein in the vicinity of RyR1 or to induce structural changes in the triadic junction by altering membrane curvature (39) that would then be responsible for the observed effects.

ACKNOWLEDGEMENTS

This work was supported by grants from Centre National de la Recherche Scientifique (CNRS), Université Lyon 1, Association Française contre les Myopathies (AFM), Hubert Curien Partnership Balaton (TeT_10-1-2011-0723) and OTKA K107765. E.G.R. was a recipient of a fellowship from the Spanish Ministry of Education and Science (MEC, José Castillejo Program). We thank Bruno Allard for critical comments on the manuscript and helpful discussion.

REFERENCES

1. Di Paolo G, De Camilli P (2006). Phosphoinositides in cell regulation and membrane dynamics. *Nature.* **443**, 651-657.
2. Suh BC, Hille B (2008). PIP2 is a necessary cofactor for ion channel function: how and why? *Annu Rev Biophys* **37**, 175-195.
3. Logothetis DE, Petrou VI, Adney SK, Mahajan R (2010). Channelopathies linked to plasma membrane phosphoinositides. *Pflugers Arch* **460**, 321-341.
4. Lanner JT, Georgiou DK, Joshi AD, Hamilton SL (2010). Ryanodine receptors: structure, expression, molecular details, and function in calcium release. *Cold Spring Harb Perspect Biol.* **2**, a003996.
5. Hannon JD, Lee NK, Yandong C, Blinks JR (1992).Inositol trisphosphate (InsP3) causes contraction in skeletal muscle only under artificial conditions: evidence that Ca^{2+} release can result from depolarization of T-tubules. *J Muscle Res Cell Motil* **13**, 447-456.
6. Kobayashi M, Muroyama A, Ohizumi Y (1989). Phosphatidylinositol 4,5-bisphosphate enhances calcium release from sarcoplasmic reticulum of skeletal muscle. *Biochem Biophys Res Commun* **163**, 1487-1491.
7. Chu A, Stefani E (1991). Phosphatidylinositol 4,5-bisphosphate-induced Ca^{2+} release from skeletal muscle sarcoplasmic reticulum terminal cisternal membranes. Ca^{2+} flux and single channel studies. *J Biol Chem* **266**, 7699-7705.
8. Ohizumi Y, Hirata Y, Suzuki A, Kobayashi M (1999). Two novel types of calcium release from skeletal sarcoplasmic reticulum by phosphatidylinositol 4,5-biphosphate. *Can J Physiol Pharmacol* **77**, 276-285.
9. Bolis A, Zordan P, Coviello S, Bolino A (2007). Myotubularin-related (MTMR) phospholipid phosphatase proteins in the peripheral nervous system. *Mol Neurobiol* **35**, 308-316.
10. Laporte J, Hu LJ, Kretz C, Mandel JL, Kioschis P, Coy JF, Klauck SM, Poustka A, Dahl N (1996). A gene mutated in X-linked myotubular myopathy defines a new putative tyrosine phosphatase family conserved in yeast. *Nat Genet* **13**, 175-182.
11. Pierson CR, Tomczak K, Agrawal P, Moghadaszadeh B, Beggs AH (2005). X-linked myotubular and centronuclear myopathies. *J Neuropathol Exp Neurol* **64**, 555-564.
12. Al-Qusairi L, Weiss N, Toussaint A, Berbey C, Messaddeq N, Kretz C, Sanoudou D, Beggs AH, Allard B, Mandel JL, Laporte J, Jacquemond V, Buj-Bello A (2009). T-tubule disorganization and defective excitation-contraction coupling in muscle fibers lacking myotubularin lipid phosphatase. *Proc Natl Acad Sci U S A.* **106,**18763-18768.
13. Dowling JJ, Vreede AP, Low SE, Gibbs EM, Kuwada JY, Bonnemann CG, Feldman EL (2009). Loss of myotubularin function results in T-tubule disorganization in zebrafish and human myotubular myopathy. *PLoS Genet* **5**, e1000372.
14. Dowling JJ, Low SE, Busta AS, Feldman EL (2010). Zebrafish MTMR14 is required for excitation-contraction coupling, developmental motor function and the regulation of autophagy. *Hum Mol Genet* **19**, 2668-2681.
15. Monnier N, Ferreiro A, Marty I, Labarre-Vila A, Mezin P, Lunardi J (2003). A homozygous splicing mutation causing a depletion of skeletal muscle RYR1 is associated with multi-minicore disease congenital myopathy with ophthalmoplegia. *Hum. Mol. Genet.* **12**, 1171-1178.
16. Zhou H, Yamaguchi N, Xu L, Wang Y, Sewry C, Jungbluth H, Zorzato F, Bertini E, Muntoni F, Meissner G, Treves S (2006). Characterization of recessive RYR1 mutations in core myopathies. *Hum Mol Genet* **15**, 2791-2803.
17. Zhou H, Jungbluth H, Sewry CA, Feng L, Bertini E, Bushby K, Straub V, Roper H, Rose MR, Brockington M, Kinali M, Manzur A, Robb S, Appleton R, Messina S, D'Amico A,

Quinlivan R, Swash M, Müller CR, Brown S, Treves S, Muntoni F (2007). Molecular mechanisms and phenotypic variation in RYR1-related congenital myopathies. *Brain* **130**, 2024-2036.

18. Zhou H, Lillis S, Loy RE, Ghassemi F, Rose MR, Norwood F, Mills K, Al-Sarraj S, Lane RJ, Feng L, Matthews E, Sewry CA, Abbs S, Buk S, Hanna M, Treves S, Dirksen RT, Meissner G, Muntoni F, Jungbluth H (2010). Multi-minicore disease and atypical periodic paralysis associated with novel mutations in the skeletal muscle ryanodine receptor (RYR1) gene. *Neuromuscul Disord* **20**, 166-173.
19. Shen J, Yu WM, Brotto M, Scherman JA, Guo C, Stoddard C, Nosek TM, Valdivia HH, Qu CK (2009). Deficiency of MIP/MTMR14 phosphatase induces a muscle disorder by disrupting Ca^{2+} homeostasis. *Nat Cell Biol* **11**, 769-776.
20. Romero-Suarez S, Shen J, Brotto L, Hall T, Mo C, Valdivia HH, Andresen J, Wacker M, Nosek TM, Qu CK, Brotto M (2010). Muscle-specific inositide phosphatase (MIP/MTMR14) is reduced with age and its loss accelerates skeletal muscle aging process by altering calcium homeostasis. *Aging* **2**, 504-513.
21. Jacquemond V (1997). Indo-1 fluorescence signals elicited by membrane depolarization in enzymatically isolated mouse skeletal muscle fibers. *Biophys J* **73**, 920-928.
22. Csernoch L, Bernengo JC, Szentesi P, Jacquemond V (1998). Measurements of intracellular Mg^{2+} concentration in mouse skeletal muscle fibers with the fluorescent indicator mag-indo-1. *Biophys J* **75**, 957-967.
23. Collet C, Csernoch L, Jacquemond V (2003). Intramembrane charge movement and L-type calcium current in skeletal muscle fibers isolated from control and mdx mice. *Biophys J* **84**, 251-265.
24. Pouvreau S, Jacquemond V (2005). Nitric oxide synthase inhibition affects sarcoplasmic reticulum Ca^{2+} release in skeletal muscle fibres from mouse. *J Physiol* **567**, 815-728.
25. Collet C, Pouvreau S, Csernoch L, Allard B, Jacquemond V (2004). Calcium signaling in isolated skeletal muscle fibers investigated under "Silicone Voltage-Clamp" conditions. *Cell Biochem Biophys* **40**, 225-236.
26. Pouvreau S, Csernoch L, Allard B, Sabatier JM, De Waard M, Ronjat M, Jacquemond V (2006). Transient loss of voltage control of Ca^{2+} release in the presence of maurocalcine in skeletal muscle. *Biophys J* **91**, 2206-2215.
27. Cheng H, Lederer WJ, Cannell MB (2003). Calcium sparks: elementary events underlying excitation-contraction coupling in heart muscle. *Science* **262**, 740-744.
28. Harkins AB, Kurebayashi N, Baylor SM (1993). Resting myoplasmic free calcium in frog skeletal muscle fibers estimated with fluo-3. *Biophys J* **65**, 865-881.
29. Csernoch L, Pouvreau S, Ronjat M, Jacquemond V (2008). Voltage-activated elementary calcium release events in isolated mouse skeletal muscle fibers. *J Membr Biol* **226**, 43-55.
30. Szabó LZ, Vincze J, Csernoch L, Szentesi P (2010). Improved spark and ember detection using stationary wavelet transforms. *J Theor Biol* **264**, 1279-1292.
31. Gouadon E, Schuhmeier RP, Ursu D, Anderson AA, Treves S, Zorzato F, Lehmann-Horn F, Melzer W (2006). A possible role of the junctional face protein JP-45 in modulating Ca^{2+} release in skeletal muscle. *J Physiol* **572**, 269-280.
32. Kirsch WG, Uttenweiler D, Fink RH (2001). Spark- and ember-like elementary Ca^{2+} release events in skinned fibres of adult mammalian skeletal muscle. *J Physiol* **537**, 379-389.
33. Lukács B, Sztretye M, Almássy J, Sárközi S, Dienes B, Mabrouk K, Simut C, Szabó L, Szentesi P, De Waard M, Ronjat M, Jóna I, Csernoch L (2008). Charged surface area of maurocalcine determines its interaction with the skeletal ryanodine receptor. *Biophys J* **95**, 3497-3509.

34. Kong D, Dan S, Yamazaki K, Yamori T (2010). Inhibition profiles of phosphatidylinositol 3-kinase inhibitors against PI3K superfamily and human cancer cell line panel JFCR39. *Eur J Cancer* **46**, 1111-1121.
35. Ogawa Y, Harafuji H (1989). Ca-release by phosphoinositides from sarcoplasmic reticulum of frog skeletal muscle. *J Biochem* **106**, 864-867.
36. Lemmon MA (2008). Membrane recognition by phospholipid-binding domains. *Nat Rev Mol Cell Bio* **9**, 99-111.
37. Bunce CM, French PJ, Allen P, Mountford JC, Moor B, Greaves MF, Michell RH, Brown G (1993). Comparison of the levels of inositol metabolites in transformed haemopoietic cells and their normal counterparts. *Biochem J* **289**, 667-673.
38. Eisenberg BR (1983). Quantitative ultrastructure of mammalian skeletal muscle. *In Handbook of Physiology (Peachey, L. D., Adrian, R. H. & Geiger, S. R., eds) sect 10: Skeletal muscle,* Williams & Wilkins, Baltimore, **3**, 73–112.
39. Amoasii L, Hnia K, Chicanne G, Brech A, Cowling BS, Müller MM, Schwab Y, Koebel P, Ferry A, Payrastre B, Laporte J (2013). Myotubularin and PtdIns3P remodel the sarcoplasmic reticulum in muscle in vivo. *J Cell Sci* (in press).

FIGURE TITLES AND LEGENDS

Figure 1. Voltage-activated Ca^{2+} release in muscle fibers injected with PtdIns*P*s. The left panel shows the mean (± S.E.M., grey shading) indo-1 saturation signal measured in the groups of muscle fibers injected with, from top to bottom, indo-1 with no PtdIns*P* (n=16) and indo-1 with PtdIns(3,5)P_2 (n=8), PtdIns(3)*P* (n=8), PtdIns(5)*P* (n=7), PtdIns (n=6), respectively. The voltage-clamp pulse protocol is shown at the top. The voltage-dependence of mean values for peak Ca^{2+} release in each condition is shown on the right, next to each corresponding indo-1 trace. The trace superimposed to each set of data points corresponds to a Boltzmann function calculated with the mean parameters obtained from an individual fit of the function to the data points in each fiber.

Figure 2. Non-linear changes in voltage-activated membrane current in muscle fibers injected with PtdIns*P*s. *A*, enlarged view of the voltage-clamp pulses used as stimulation protocol in Fig. 1. *B*, mean (± S.E.M., grey shading) changes in membrane current elicited by the successive voltage-clamp pulses in the batch of control fibers. In each fiber, membrane current traces were corrected from the passive linear components and normalized to the capacitance. *C*, voltage-dependence of mean values for *on* charge and for the membrane current at the end of the depolarizing pulse in the different groups of fibers. Values from control fibers (filled circles) are reported in each panel. See text and Material and Methods for details.

Figure 3. Effect of PtdIns*P*s on spontaneous elementary Ca^{2+} release events in permeabilised muscle fibers. *A*, cumulated ECRE activity recorded with fluo-3 over a series of 200 consecutive confocal frames in fibers equilibrated with the indicated PtdIns*P* and in control fibers. *B*, mean values for the measured ECRE parameters in the different group of fibers. The number of fibers in the presence of a given PtdIns*P* and in the corresponding control group was 27 and 28 (PtdIns(3,5)P_2), 29 and 28 (PtdIns(3)*P*), 36 and 40 (PtdIns(5)*P*), 12 and 11(PtdIns), respectively. All images are 84×84 µm.

Figure 4. Voltage-dependent Ca^{2+} release in fibers injected with the PtdIns-3 kinase inhibitor LY294002. *A*, voltage-clamp pulse protocol. *B*, mean (± S.E.M., grey shading) indo-1 saturation signal measured in fibers injected with LY294002 (n=6) and in the corresponding batch of control fibers (n=6). *C*, voltage-dependence of mean peak values of Ca^{2+} release in the two groups of fibers. The trace superimposed to each set of data points corresponds to a Boltzmann function calculated with the mean parameters obtained from an individual fit of the function to the data points in each fiber. Mean values for maximum peak Ca^{2+} release, voltage of half-activation and steepness factor were 32.6 ± 1 µM.ms^{-1}, -5.8 ± 2 mV, 6.4 ± 0.3 mV and 32.1 ± 2 µM.ms^{-1}, -5.3 ± 3 mV, 6.7 ± 0.2 mV in control and LY294002-injected fibers, respectively.

Figure 5. Expression of the PtdIns*P*s phosphatase MTM1 in mouse muscle fibers. *A-B*, representative confocal images of the mCherry fluorescence from fibers expressing mCherry-tagged MTM1. *C*, mCherry fluorescence profile along the *x* axis of the yellow box in *B*. *D-F*, co-localization of mCherry and di-8-anneps (green) fluorescence. Scale bars in the images all correspond to 10 µm.

Figure 6. Voltage-dependent Ca^{2+} release in fibers expressing mCherry-tagged MTM1. *A*, pulse protocol. *B*, mean (± S.E.M., grey shading) indo-1 saturation trace from control fibers

(n=11) and from mCherry-MTM1 positive fibers (n=11). *C*, corresponding mean voltage-dependence of peak Ca^{2+} release in the two sets of fibers.

Figure 1

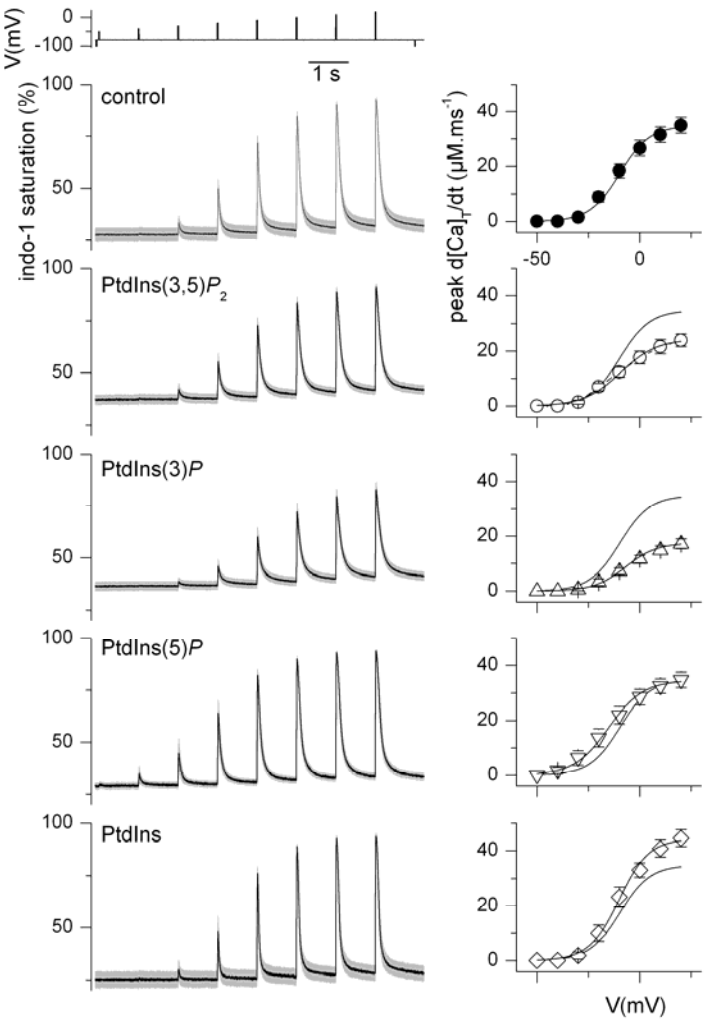
V(mV)
0
-100
1 s
indo-1 saturation (%)
100
50
control
PtdIns(3,5)P_2
PtdIns(3)P
PtdIns(5)P
PtdIns
peak d[Ca]$_i$/dt (μM.ms^{-1})
40
20
0
-50
V(mV)

Figure 2

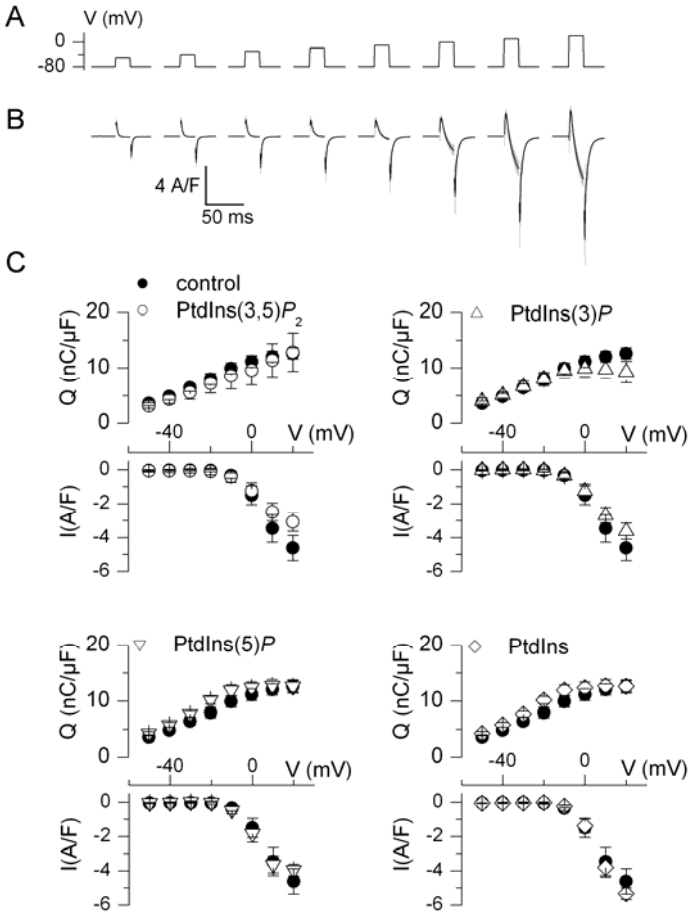
A
V (mV)
0
-80
B
4 A/F
50 ms
C
control
PtdIns(3,5)P2
PtdIns(3)P
PtdIns(5)P
PtdIns
Q (nC/µF)
I(A/F)
V (mV)
-40
0

Figure 3

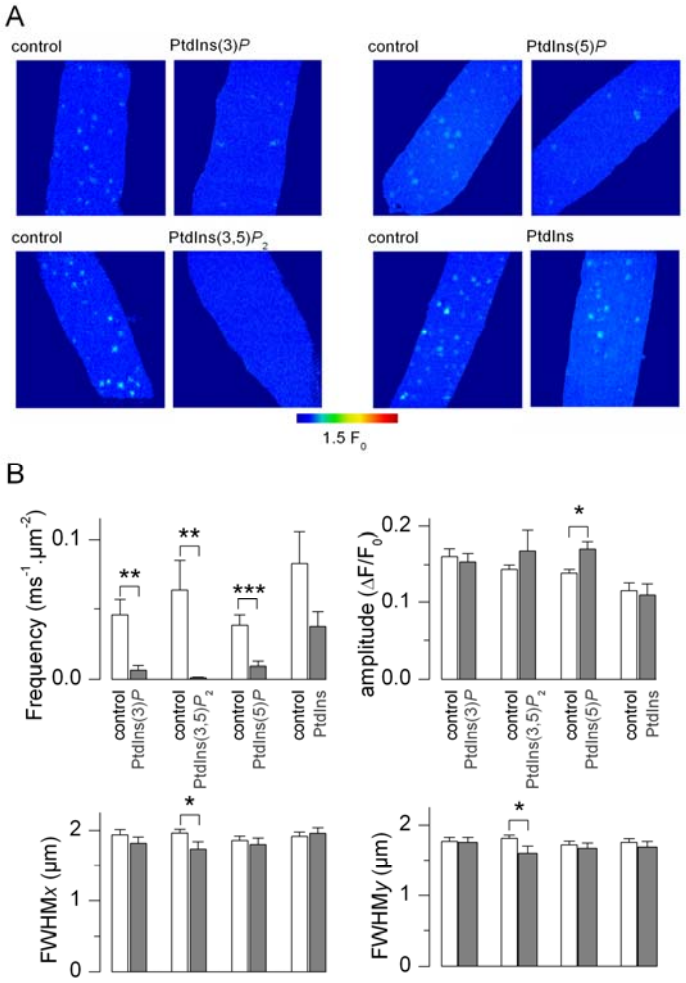
A
control
PtdIns(3)P
control
PtdIns(5)P
control
PtdIns(3,5)P2
control
PtdIns
1.5 F0
B
Frequency (ms-1.µm-2)
amplitude (ΔF/F0)
FWHMx (µm)
FWHMy (µm)
control
PtdIns(3)P
PtdIns(3,5)P2
PtdIns(5)P
PtdIns

Figure 4

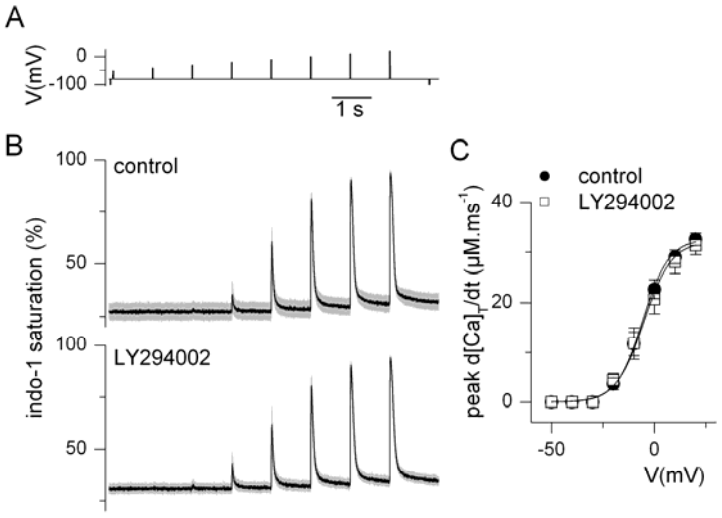
A
V(mV)
0
-100
1 s
B
control
LY294002
indo-1 saturation (%)
100
50
C
control
LY294002
peak d[Ca]i/dt (μM.ms-1)
40
20
0
-50
0
V(mV)

Figure 5

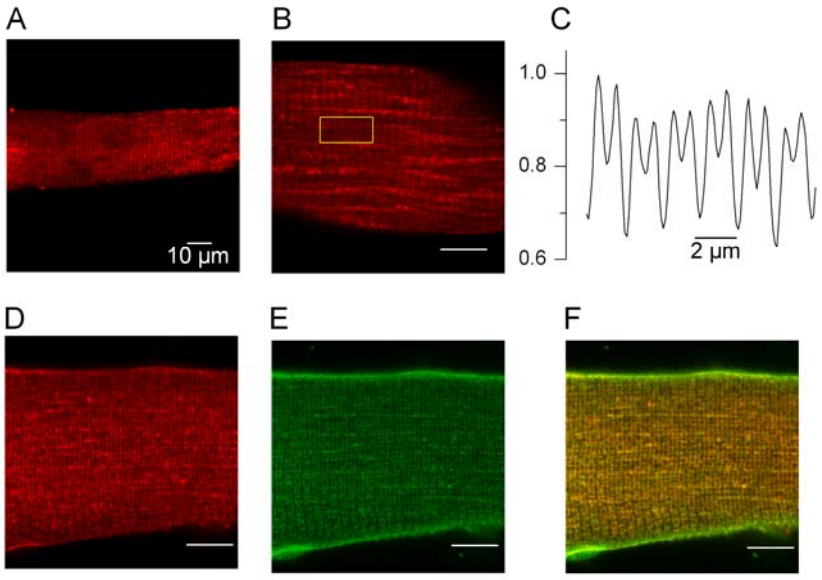

Figure 6

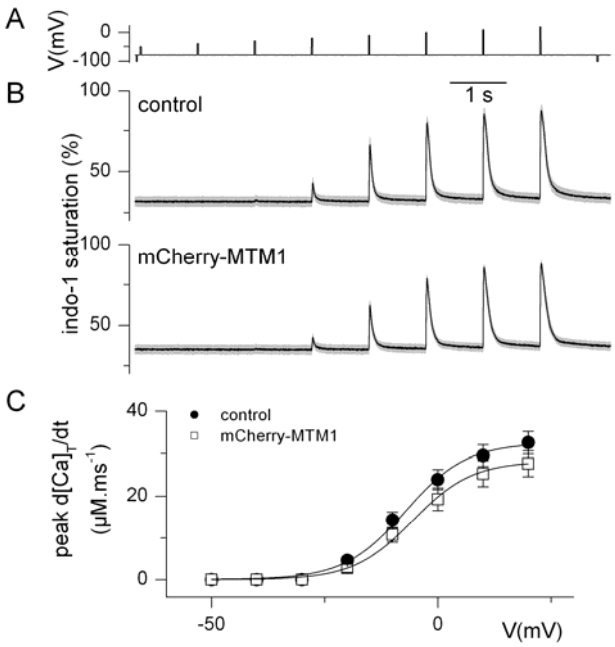
A
V(mV)
0
-100
B
100
control
1 s
indo-1 saturation (%)
50
100
mCherry-MTM1
50
C
40
control
mCherry-MTM1
peak d[Ca]i/dt
(µM.ms-1)
20
0
-50
0
V(mV)